JACC: ASIA VOL. 2, NO. 7, 2022

ORIGINAL RESEARCH

Clinical and Predictive Value of Computed Tomography Angiography in High-Altitude Pulmonary Hypertension

Yanxi Zeng, MD,[a,b,*] Qing Yu, MD,[b,*] Nuerbiyemu Maimaitiaili, MD,[b] Bingyu Li, MD,[b] Panjin Liu, MD,[a] Yongzhi Hou, MD,[c] Mima, MD,[a] Cirenguojie, MD,[d] Gupta Sumit, PHD,[e] Dejizhuoga, MD,[a,b] Yong Liu, MD,[f] Wenhui Peng, MD, PHD[a,b]

ABSTRACT

BACKGROUND High-altitude pulmonary hypertension (HAPH), as the group 3 pulmonary hypertension, has been less studied so far. The limited medical conditions in the high-altitude plateau are responsible for the delay of the clinical management of HAPH.

OBJECTIVES This study aims to identify the imaging characteristics of HAPH and explore noninvasive assessment of mean pulmonary arterial pressure (mPAP) based on computed tomography angiography (CTA).

METHODS Twenty-five patients with suspected HAPH were enrolled. Right heart catheterization (RHC) and pulmonary angiography were performed. Echocardiography and CTA image data were collected for analysis. A multivariable linear regression model was fit to estimate mPAP ($mPAP_{predicted}$). A Bland-Altman plot and pathological analysis were performed to assess the diagnostic accuracy of this model.

RESULTS Patients with HAPH showed slow blood flow and coral signs in lower lobe pulmonary artery in pulmonary arteriography, and presented trend for dilated pulmonary vessels, enlarged right atrium, and compressed left atrium in CTA (P for trend <0.05). The left lower pulmonary artery-bronchus ratio (odds ratio: 1.13) and the ratio of right to left atrial diameter (odds ratio: 1.09) were significantly associated with HAPH, and showed strong correlation with $mPAP_{RHC}$, respectively ($r = 0.821$ and $r = 0.649$, respectively; all $P < 0.0001$). The $mPAP_{predicted}$ model using left lower artery-bronchus ratio and ratio of right to left atrial diameter as covariates showed high correlation with $mPAP_{RHC}$ ($r = 0.907$; $P < 0.0001$). Patients with predicted HAPH also had the typical pathological changes of pulmonary hypertension.

CONCLUSIONS Noninvasive mPAP estimation model based on CTA image data can accurately fit $mPAP_{RHC}$ and is beneficial for the early diagnosis of HAPH. (JACC: Asia 2022;2:803-815) © 2022 The Authors. Published by Elsevier on behalf of the American College of Cardiology Foundation. This is an open access article under the CC BY-NC-ND license (http://creativecommons.org/licenses/by-nc-nd/4.0/).

From the [a]Department of Cardiology, Shigatse People's Hospital, Tibet, China; [b]Department of Cardiology, Shanghai Tenth People's Hospital, School of Medicine, Tongji University, Shanghai, China; [c]Department of Ultrasound, Shigatse People's Hospital, Tibet, China; [d]Department of Radiology, Shigatse People's Hospital, Tibet, China; [e]Department of Radiology, Brigham and Women's Hospital, Harvard Medical School, Boston, Massachusetts, USA; and the [f]Department of Radiology, Shanghai Tenth People's Hospital, School of Medicine, Tongji University, Shanghai, China. *Drs Zeng and Yu contributed equally and share the first authorship.

The authors attest they are in compliance with human studies committees and animal welfare regulations of the authors' institutions and Food and Drug Administration guidelines, including patient consent where appropriate. For more information, visit the Author Center.

Manuscript received April 27, 2022; revised manuscript received September 6, 2022, accepted September 7, 2022.

ISSN 2772-3747 https://doi.org/10.1016/j.jacasi.2022.09.014

JACC: ASIA, VOL. 2, NO. 7, 2022
DECEMBER 2022:803–815

ABBREVIATIONS AND ACRONYMS

ABR = pulmonary artery-bronchus ratio

HAPH = high-altitude pulmonary hypertension

LVEF = left ventricle ejection fraction

mPAP = mean pulmonary arterial pressure

PASP = pulmonary arterial systolic pressure

PH = pulmonary hypertension

RHC = right heart catheterization

rPA = the ratio of main pulmonary artery to aorta diameter

rRLA = the ratio of right to left atrial diameter

TRPG = tricuspid regurgitation pressure gradient

Pulmonary hypertension (PH) is defined as mean pulmonary arterial pressure (mPAP) ≥25 mm Hg at rest or >30 mm Hg with exercise as assessed by right heart catheterization (RHC) and is classified into 5 groups: group 1 PH, pulmonary arterial hypertension; group 2 PH, PH due to left heart disease; group 3 PH, PH due to lung diseases and/or hypoxia; group 4 PH, chronic thromboembolic pulmonary hypertension; and group 5 PH, PH with unclear and/or multifactorial aetiologies.[1] Persistent elevation of pulmonary arterial pressure leads to irreversible pulmonary vascular remodeling, which would cause a poor prognosis if left untreated and eventually evolve into right heart failure.[2,3] Thus, early diagnosis and therapeutic intervention are crucial to improve outcomes.

It is estimated that more than 140 million people reside in the high-altitude plateau areas, which is defined as being at least 2,500 meters above sea level.[4] In addition, approximately 40 million temporary visitors travel to mountain areas annually.[5] The living environment and physiological conditions between the plain (<1,000 m) and high-altitude plateau (>2,500 m) residents are different[6]; lifelong exposure to hypoxia may lead to progressive incapacitating syndrome chronic mountain sickness, which is characterized by severe symptomatic excessive erythrocytosis and PH due to hypoxemia.[5,7] In advanced cases, the condition may progress to cor pulmonale and congestive heart failure.[8] High-altitude pulmonary hypertension (HAPH) due to chronic exposure to high altitude is a designated subset of PH, PH due to lung diseases and/or hypoxia (group 3 PH).[9] However, RHC, as the gold standard for diagnosis, is rarely performed because of the limitations of technology and equipment in the high-altitude plateau areas.[10] In addition, echocardiographic measurement of pulmonary arterial systolic pressure (PASP) is not performed routinely due to high variability and observer dependence.[11] As a relatively objective and frequently clinically performed imaging examination, computed tomography angiography (CTA) has a higher data reliability compared with echocardiography.[1] The purpose of this study was to explore the imaging characteristics of patients with HAPH via pulmonary angiography and CTA, and to increase diagnostic accuracy based on the parameter of noninvasive imaging, further improving the early diagnosis and treatment of PH in plateau areas.

METHODS

STUDY DESIGN AND POPULATION. The institutional review board of Shigatse People's Hospital approved this prospective study, and informed consent was obtained. The inclusion criteria were the following: 1) male or female patient between the ages of 21 and 85 years; 2) admitted in Shigatse People's Hospital between August 2020 and August 2021; 3) history of residence in the plateau for more than 20 years; 4) initial diagnosis suggestive PH (symptoms, signs, history, electrocardiogram, and chest radiograph); 5) echocardiographic PASP more than 40 mm Hg; and 6) no contraindications of CTA/RHC and had provided informed consent. Records of all patients undergoing transthoracic echocardiography, CTA or computed tomography (CT), arterial blood gases, pulmonary arteriography, and RHC for the initial diagnostic workup of suspected HAPH were reviewed. The exclusion criteria of this study included the following: signs of chronic thromboembolic disease in CTA, contraindications of RHC, partial pressure of oxygen in arterial blood ≥83 mm Hg, and history of left heart disease including systolic dysfunction (ie, dilated or ischemic cardiomyopathy), diastolic dysfunction (ie, hypertrophic cardiomyopathy), and valvular disease.[8] Furthermore, the interval between the patients' CTA and RHC were more than 30 days, and those who did not measure echocardiographic PASP were excluded (Supplemental Figure 1). Patients with HAPH were diagnosed with $mPAP_{RHC}$ >30 mm Hg according to the Qinghai criteria published by the International Society for Mountain Medicine in 2005.[12]

PULMONARY ARTERIOGRAPHY AND CTA/CT ACQUISITION. Scans of 25 patients had been acquired at our institution on United Imaging scanners and were performed in a supine position in inspiratory breath-hold. Scanning parameters were as follows: tube voltage of 120 kVp, tube current 300 mA, tube rotation time 0.3s, and collimator width 64 mm × 0.625 mm. Scan plans were made prospectively and ranging from the apex pulmonis to the diaphragm. Iodinated contrast agent (iomeprol, 400 mgL/mL, Bracco Sine, China) was injected through the median cubital vein with double-syringe power injector. The intelligent tracking mode was used and flushing with 20 mL saline at 4 mL/s before scanning. A 60-mL contrast agent was injected at 4 mL/s followed by a saline bolus of 50 mL. The scanning was triggered when the density of the main pulmonary artery reached the preset peak 80 HU.[13] On the 4-chamber transversal view, the widest part of

atrium perpendicular to the long axis was measured as atrial diameter, which were also measured in 3 adjacent slices for verification. The diameter of the left lower bronchus was measured at the junction with the left main bronchus, and the diameter of the accompanying artery was measured at the same slice and the artery-bronchus ratio (ABR) was calculated.

ECHOCARDIOGRAPHY. The peak tricuspid regurgitation velocity, the main pulmonary artery diameter, the vertical/transverse diameter of left/right atrium/ventricle and the left ventricle ejection fraction (LVEF) were measured by echocardiography using the guideline from the American Society of Echocardiography.[14] The pressure gradient between the right atrium and ventricle was estimated based on the tricuspid regurgitation pressure gradient (TRPG) calculated with the modified Bernoulli equation.[15] The inferior vena cava diameter and collapsibility estimated the right atrial pressure. PASP was calculated based on the estimated pressure gradient and right atrial pressure.[16]

RHC. RHC was performed according to standard procedures by an interventional cardiologist with more than 5 years of experience.[1,5] In short, an introducer sheath was placed in the right femoral vein. A JR 4.0 catheter (Cordis) was introduced to the pulmonary artery under local anesthesia to measure mPAP by RHC ($mPAP_{RHC}$). $mPAP_{RHC}$ was recorded in the main pulmonary artery above the pulmonary valve, and systolic (diastolic) pressures of right ventricle, right atrium, and superior vena cava were measured using a standard technique image analysis.[17]

HISTOLOGY AND IMMUNOHISTOLOGY. For histological analysis, lung tissue samples were fixed in 10% formalin, dehydrated, and paraffin-embedded for sectioning and then used for hematoxylin-and-eosin staining and immunohistochemical staining. For α-smooth muscle actin (SMA) immunohistochemical staining, sections were incubated overnight with primary antibody against α-SMA (19245S, Cell Signaling Technology) Image J (V1.49, NIH) software was used for vascular thickness and image areas analysis. Wall thickness was calculated as the ratio of the difference between the external and internal diameters to the external diameter of the pulmonary artery. All lung tissues were collected intraoperatively with surgical indications, informed consent and the approval of the ethics committee of Shigatse People's Hospital, and the pathological diagnosis was confirmed by the pathologists according to the pathological sections. The characteristics and pathological diagnosis of 9 plateau residents are shown in Supplemental Materials. Patients without surgical indications were excluded for pathological analysis.

STATISTICAL ANALYSIS. Characteristics of the study patients were described by $mPAP_{RHC}$, and normal distribution of measurements was tested with the Shapiro-Wilk test. Data were presented as mean ± SD or median (IQR) if not normally distributed. Categorical data were presented as absolute number (percentage). Group differences were assessed by one-way analysis of variance, and Kruskal-Wallis H test or Fisher exact test as appropriate. The linear trend between continuous variables and the different level of $mPAP_{RHC}$ was evaluated by linear regression analysis. The trend between dichotomous variables' positive or negative rate and the elevated $mPAP_{RHC}$ was evaluated by the Cochran-Armitage trend test. Parameters with statistically significant differences were included in subsequent correlation and logistic regression analysis. Correlation between parameters and $mPAP_{RHC}$ was analyzed using Pearson's/Spearman's correlation. The univariate logistic regression analysis was used to calculate odds ratios (ORs) and 95% CIs. Difference, correlation, and regression analysis were used to filter variables into the model. A forward stepwise multivariable linear regression analysis was performed to generate a numerical model for noninvasive mPAP estimation ($mPAP_{predicted}$) with a required variable significance of 0.05 in the model, and a cut-off value of 0.1 for exclusion. Bland-Altman analyses were performed to assess the diagnostic consistency of mPAP from the estimation model with that of RHC. A receiver operating characteristic (ROC) curve was constructed and the area under the ROC curve was calculated to assess the diagnostic performance to detect HAPH by estimation model. All the analyses were performed using R (v.4.1.2) and SPSS (v.26.0). The 2-sided $P < 0.05$ was considered statistically significant.

RESULTS

BASIC CLINICAL CHARACTERISTICS OF THE STUDY POPULATION. A total of 25 suspected HAPH patients were enrolled in our study (mean age, 64 years; males, 60%), with average $mPAP_{RHC}$ to be 46 mm Hg ranging from 18 to 101 mm Hg. Of these patients, 7 (28%), 13 (52%), and 5 (20%) were with $mPAP_{RHC}$ of ≤30 mm Hg, 30 to 60 mm Hg, and >60 mm Hg, respectively.[18] There were no significant differences in sex and age among all groups. Patients with HAPH were more prone to have elevated transaminase, uric acid, and creatine phosphokinase-MB (P for trend <0.05) (**Table 1**), which indicates right cardiac insufficiency with increased $mPAP_{RHC}$. The between-group

TABLE 1 Characteristics of Clinical Laboratory Indicators

		3 Levels of Predicted mPAP					
	Total	≤30 (n = 7)	30-60 (n = 13)	>60 (n = 5)	Chi-Square/F/H	*P* Value	*P* Value for Trend
Male	15 (60)	4 (57)	6 (46)	5 (100)			
Female	10 (40)	3 (43)	7 (54)	0 (0)	4.271	0.150	0.192
Age, y	64 (42-70)	52 (39-66)	64 (46-71)	66 (42-76)	1.548	0.461	0.401
CRP, mg/L	1.38 (0.20-3.60)	0.20 (0.20-0.61)	1.68 (0.64-8.18)	2.94 (0.69-6.01)	2.904	0.234	0.998
RBC, $\times10^{12}$/L	5.47 ± 1.02	5.20 ± 1.08	5.46 ± 1.12	5.90 ± 0.65	0.651	0.531	0.267
WBC, $\times10^{9}$/L	5.39 (4.66-7.00)	5.11 (4.40-7.72)	5.75 (4.65-7.09)	5.39 (4.66-6.47)	0.261	0.878	0.326
Neu, %	68.5 (59.2-71.4)	67.3 (59.1-68.6)	70.4 (67.8-73.7)	58.6 (58.5-69.1)	4.694	0.096	0.538
HGB, g/L	160 ± 37	162 ± 30	147 ± 36	192 ± 30	3.195	0.061	0.144
HCT, %	50.3 ± 10.8	49.6 ± 10.8	48.0 ± 11.4	57.1 ± 7.7	1.349	0.280	0.239
ALT, U/L	30 (18-52)	31 (21-44)	21 (14-45)	60 (34-87)	6.189	0.045[a]	0.044[b]
AST, U/L	27 (23-59)	25 (21-51)	26 (23-46)	68 (47-90)	7.458	0.024[a]	0.005[b]
Albumin, g/L	40.0 (34.4-46.0)	46.6 (39.8-65.7)	38.8 (33.4-41.4)	36.4 (30.1-48.2)	5.595	0.061	0.058
TBil, μmol/L	19.7 (13.3-39.1)	15.1 (13.3-17.9)	29.4 (10.4-39.9)	30.0 (20.8-72.5)	2.623	0.269	0.052
CREA, μmol/L	84.30 ±19.58	75.09 ± 18.08	87.27 ± 19.89	89.50 ± 20.32	1.111	0.347	0.220
UA, μmol/L	340 (255-492)	260 (187-383)	302 (256-409)	622 (508-663)	10.839	0.004[a]	<0.001[b]
BUN, mmol/L	4.89 ± 2.36	4.54 ± 1.34	4.54 ± 1.96	6.29 ± 4.01	1.111	0.347	0.216
NT-proBNP, pg/L	2470 (791-3,979)	175 (75-5,123)	2,811 (931-3,801)	2,470 (1,553-5,978)	1.922	0.382	0.353
PT, s	13.48 ± 3.47	12.03 ± 2.94	13.29 ± 2.45	16.00 ± 5.43	2.139	0.142	0.053
FIB, g/L	2.00 (1.76-2.60)	2.50 (2.30-2.81)	2.00 (1.65-2.42)	1.86 (1.60-2.44)	2.959	0.228	0.282
D-D dimer, mg/L	0.55 (0.38-1.57)	0.33 (0.23-0.45)	0.73 (0.50-2.30)	0.62 (0.46-2.09)	6.323	0.042[a]	0.454
PH	7.43 (7.40-7.46)	7.42 (7.40-7.45)	7.43 (7.41-7.47)	7.42 (7.37-7.45)	1.502	0.472	0.876
PaO_2, mm Hg	51 (48-58)	50 (47-56)	51 (48-67)	55 (38-58)	0.587	0.746	0.932
$PaCO_2$, mm Hg	32 (28-37)	32 (30-32)	35 (31-41)	26 (22-34)	4.175	0.124	0.512
BE, mmol/L	-3.7 (-5.0 to -0.5)	-3.7 (-6.0 to -2.0)	-2.0 (-4.5 to -2.5)	-5.0 (-13 to -3.5)	4.000	0.135	0.524
SaO_2, %	83.9 ± 9.6	84.7 ± 3.0	83.8 ± 12.0	83.0 ± 10.4	0.041	0.960	0.781
HCO_3^-, mmol/L	21.41 (19.60-24.3)	21.4 (21.2-21.8)	24.1 (20.1-27.0)	18.6 (12.4-21.2)	4.363	0.113	0.156
TC, mmol/L	3.39 ± 0.83	3.61 ± 0.85	3.35 ± 0.85	3.17 ± 0.87	0.417	0.664	0.384
TG, mmol/L	0.96 ± 0.27	1.11 ± 0.29	0.87 ± 0.26	0.97 ± 0.26	1.840	0.182	0.391
HDL-C, mmol/L	1.11 ± 0.31	1.16 ± 0.26	1.14 ± 0.31	0.99 ± 0.41	0.489	0.602	0.377
LDL-C, mmol/L	1.94 (1.53-2.35)	2.02 (1.57-2.13)	1.92 (1.47-2.56)	1.85 (1.56-2.42)	0.250	0.883	0.745
Blood glucose, mmol/L	4.40 (4.04-4.88)	4.42 (3.91-5.27)	4.50 (4.07-4.98)	4.17 (3.80-4.47)	1.700	0.427	0.176
CK-MB, ng/mL	1.93 (1.29-3.95)	1.05 (0.56-2.15)	2.22 (1.40-3.95)	4.62 (1.42-6.16)	6.003	0.050[a]	0.024[b]
Myoglobin, ng/mL	46.7 (33.6-63.1)	52.7(33.8-52.8)	40.0 (29.7-56.1)	68.0 (29.2-107.0)	1.150	0.563	0.306
cTnT, ng/mL	0.42 (0.25-0.51)	0.45 (0.23-0.45)	0.38 (0.21-0.64)	0.44 (0.20-0.51)	0.042	0.979	0.806
HbA1c, %	5.70 (5.39-6.50)	5.48 (4.10-5.70)	6.20 (5.48-6.86)	6.34 (5.41-6.8)	2.795	0.247	0.185

Values are n (%), median (IQR), or mean ± SD. Group differences were assessed by 1-way ANOVA, Fisher exact test, or Kruskal-Wallis H tests. [a]$P < 0.05$: the group difference assessed by Kruskal-Wallis H test was significant. [b]$P < 0.05$: the linear association between continuous variables was significant, and the elevated $mPAP_{RHC}$ is evaluated by linear regression analysis.

ALT = alanine aminotransferase; ANOVA = analysis of variance; AST = aspartate aminotransferase; BE = base excess; BUN = Blood urea nitrogen; CK-MB = creatine phosphokinase-MB; CREA = creatinine; CRP = C-reactive protein; cTnT = cardiac troponin T; FIB = fibrinogen; HCO_3^- = bicarbonate concentration; HCT = red blood cell specific volume; HDL-C = high-density lipoprotein cholesterol; HGB = hemoglobin; HbA1C = glycosylated hemoglobin; LDL-C = low-density lipoprotein cholesterol; mPAP = mean pulmonary arterial pressure; Neu = neutrophilic granulocyte percentage; NT-proBNP = N-terminal pro-B-type natriuretic peptides; $PaCO_2$ = carbon dioxide partial pressure; PaO_2 = oxygen partial pressure; PH = pulmonary hypertension; PT = prothrombin time; RBC = red blood cell; RHC = right heart catheterization; SaO_2 = oxyhemoglobin saturation; TBil = total bilirubin; TC = total cholesterol; TG = triglyceride; UA = uric acid; WBC = white blood cell.

difference and 95% CI of clinical characteristics are described in Supplemental Table 1. The correlation (Supplemental Table 2) and the estimation model between lab tests and $mPAP_{RHC}$ (Supplemental Figure 2) suggested auxiliary role in clinical diagnosis.

IMAGING CHARACTERISTICS OF HAPH. As echocardiography is regarded as the initial screening method for PH, noninvasive imaging examinations were first analyzed by echocardiography and parameters are shown in **Table 2**. Participants with high $mPAP_{RHC}$ were more likely to have enlarged right ventricle in both transverse diameter (*P* for trend = 0.019) and vertical diameter (*P* for trend = 0.001), increased TRPG and PASP (*P* for trend = 0.010 and 0.009, respectively), whereas no significant differences were found in atrial and left ventricle diameter and LVEF between the 3 groups.

Next, all participants underwent pulmonary CTA, showing that participants with high $mPAP_{RHC}$ were more likely to have enlarged right atrium (*P* for trend = 0.004), dilated superior/inferior vena cava (*P* for trend = 0.008 and 0.004, respectively), main pulmonary artery (*P* for trend = 0.015), and left pulmonary artery (*P* for trend = 0.017). Furthermore, the

TABLE 2 Characteristics of Parameters of Echocardiography

			3 Levels of Predicted mPAP					
	Group	Total	≤30 (n = 7)	30-60 (n = 13)	>60 (n = 5)	Chi-Square/F/H	*P* Value	*P* Value for Trend
RATD, mm	Normal	3 (12)	2 (29)	1 (8)	0 (0)			
	Enlarge	22 (88)	5 (71)	12 (92)	5 (100)	2.181	0.271	0.123
RAVD, mm	Normal	2 (8)	2 (29)	0 (0)	0 (0)			
	Enlarge	23 (92)	5 (71)	13 (100)	5 (100)	3.960	0.103	0.053
RVTD, mm	Normal	6 (24)	4 (57)	2 (15)	0 (0)			
	Enlarge	19 (76)	3 (43)	11 (85)	5 (100)	5.171	0.065	0.019[a]
RVVD, mm	Normal	5 (20)	5 (71)	0 (0)	0 (0)			
	Enlarge	20 (80)	2 (29)	13 (100)	5 (100)	12.760	0.001[b]	0.001[a]
LATD, mm	Normal	14 (56)	5 (71)	7 (54)	2 (40)			
	Enlarge	11 (44)	2 (29)	6 (46)	3 (60)	1.255	0.663	0.281
LAVD, mm	Normal	15 (60)	5 (71)	8 (62)	2 (40)			
	Enlarge	10 (40)	2 (29)	5 (38)	3 (60)	1.263	0.660	0.295
LVEDD, mm	Normal	17 (68)	5 (71)	8 (62)	4 (80)			
	Enlarge	8 (32)	2 (29)	5 (38)	1 (20)	0.633	0.861	0.826
LVESD, mm	Enlarge	17 (68)	5 (71)	8 (62)	4 (80)			
	Normal	8 (32)	2 (29)	5 (38)	1 (20)	0.633	0.861	0.826
MPAD, mm	Enlarge	6 (24)	4 (57)	2 (15)	0 (0)			
	Normal	19 (76)	3 (43)	11 (85)	5 (100)	5.171	0.065	0.019[a]
TRPG, mm Hg		51.4 ± 24.4	35.7 ± 22.2	52.1 ± 22.1	71.8 ± 20.1	4.020	0.033[c]	0.010[d]
PASP, mm Hg		62.5 ± 24.7	47.0 ± 21.6	62.7 ± 22.6	83.8 ± 20.9	4.068	0.031[c]	0.009[d]
LVEF, %		63 (53-66)	62 (47-67)	63 (53-63)	66 (60-68)	1.520	0.468	0.268

Values are n (%), mean ± SD, or median (IQR). Group differences were assessed by 1-way ANOVA, Fisher exact test, or Kruskal-Wallis H tests. [a]*P* for trend < 0.05: the trend between dichotomous variables' positive or negative rate and the elevated $mPAP_{RHC}$ based on Cochran-Armitage trend test was significant. [b]*P* < 0.05: the group difference assessed by Fisher exact test was significant. [c]*P* < 0.05: The group difference assessed by one-way ANOVA was significant. [d]*P* for trend < 0.05: the linear association between continuous variables was significant, and the elevated $mPAP_{RHC}$ is evaluated by linear regression analysis.

LATD = transverse diameter of left atrium; LAVD = vertical diameter of left atrium; LVEDD = left ventricle end-diastolic diameter; LVEF = left ventricular ejection fraction. LVESD = left ventricle end-systolic diameter; MPAD = main pulmonary artery diameter measured by echocardiography; PASP = echocardiographic pulmonary arterial systolic pressure estimate; RATD = transverse diameter of right atrium; RAVD = vertical diameter of right atrium; RVTD = transverse diameter of right ventricle; RVVD = vertical diameter of right ventricle; TRPG = tricuspid regurgitation differential pressure; other abbreviations as in Table 1.

ratio based on the above parameters also increased with high $mPAP_{RHC}$, such as the ratio of right to left atrial diameter (rRLA), the ratio of main pulmonary artery to aorta diameter (rPA), and left lower ABR (*P* for trend <0.001) (Table 3). The vessel, bronchial, and atrial measurements obtained from CTA and CT scans are shown in Figure 1A. Compared with CTA (Figure 1A, upper), the CT image (Figure 1A, lower) was more blurred but could still be used if CTA was not available. The between-group difference and 95% CI of imaging characteristics in echocardiography and CTA is described in Supplemental Table 3.

After CTA and CT, RHC and angiography were next performed, and pulmonary angiography was adopted to further show the imaging characteristics of HAPH patients. Compared to plateau residents with normal $mPAP_{RHC}$, the blood flow of the pulmonary artery in patients with HAPH were much slower. The "coral sign" was observed more obviously in the lower pulmonary artery, which showed arterial branches increased, enlarged, and twisted with intima rough similar to coral (Figure 1B) and was in consistent with observations from CTA and CT.

IDENTIFICATION OF POTENTIAL PREDICTORS. The parameters in echocardiography and CTA were uniformly analyzed to select potential predictive variables. Pearson's/Spearman's correlation analysis of imaging measurements in relation to $mPAP_{RHC}$ showed low correlation between $mPAP_{RHC}$ and echocardiography parameters, such as TRPG (r = 0.469) and PASP (r = 0.439) (*P* < 0.05). There were moderate correlations between $mPAP_{RHC}$ and right atrial diameter (r = 0.546), superior vena cava diameter (r = 0.516), main pulmonary artery diameter (r = 0.559), and rPA (r = 0.583) (*P* < 0.05). High correlations between $mPAP_{RHC}$ and inferior vena cava diameter (r = 0.617) and rRLA (r = 0.649) were also documented (*P* < 0.001). The left lower ABR had the strongest correlation with $mPAP_{RHC}$ (r = 0.821; *P* < 0.0001) (Table 4). Above all variables, parameters of CTA had a relatively stronger correlation with $mPAP_{RHC}$ compared with those of echocardiography.

The univariate logistic regression analysis conducted by HAPH as the dependent variable showed that compared with plateau residents with normal mPAP from CTA scans, the ORs of right atrial diameter, inferior vena cava diameter, and left pulmonary

TABLE 3 Characteristics of Parameters of CTA

		3 Levels of Predicted mPAP					
	Total	≤30 (n = 7)	30-60 (n = 13)	>60 (n = 5)	F/H	*P* Value	*P* Value for Trend
RAD, mm	64.1 ± 16.3	49.4 ± 8.0	67.7 ± 14.7	75.2 ± 16.4	6.183	0.007[a]	0.004[b]
LAD, mm	38.6 ± 9.1	41.3 ± 5.5	39.2 ± 9.5	33.0 ± 11.2	1.320	0.287	0.129
SVCD, mm	29.8 ± 8.7	24.9 ± 3.2	29.4 ± 7.5	38 ± 11.9	4.284	0.027[a]	0.008[b]
IVCD, mm	23.1 ± 6.0	18.6 ± 3.0	23.3 ± 4.9	28.6 ± 7.8	5.172	0.014[a]	0.004[b]
AAD, mm	33.0 ± 4.6	34.3 ± 5.2	32.2 ± 4.9	33.2 ± 3.2	0.472	0.630	0.698
MPAD, mm	38.8 ± 7.2	34.3 ± 7.4	39.0 ± 6.6	44.4 ± 4.8	3.522	0.047[a]	0.015[b]
LPAD, mm	26.7 ± 4.8	23.1 ± 4.6	27.5 ± 4.5	29.6 ± 2.9	3.831	0.037[a]	0.017[b]
RPAD, mm	26.2 ± 4.9	24.9 ± 4.6	25.5 ± 5.3	30.0 ± 2.55	2.064	0.151	0.074
rRLA, %	162.5 (119.8-202.6)	115.7 (112.8-125.0)	167.0 (134.0-226.4)	190.0 (160.8-379.4)	11.483	0.003[c]	<0.001[b]
rSIVC, %	130.0 (116.3-150.4)	130.0 (117.7-136.4)	129.7 (103.9-160.5)	134.3 (105.9-168.4)	0.074	0.963	0.883
rPA, %	118.3 ± 19.9	100.1 ± 15.1	121.8 ± 16.4	134.5 ± 16.7	7.244	0.004[a]	<0.001[b]
Left upper ABR, %	133.3 (114.6-150.0)	133.3 (116.7-144.4)	133.3 (106.3-146.4)	150.0 (122.2-155.6)	2.062	0.357	0.423
Left lower ABR, %	154.6 (134.8-186.1)	120.0 (118.2-141.7)	154.6 (147.2-185.4)	233.3 (175.0-250.0)	14.310	<0.001[c]	<0.001[b]
Right upper ABR, %	154.9 ± 40.4	131.2 ± 33.9	154.3 ± 32.0	190.0 ± 49.5	3.841	0.037[a]	0.011[b]
Right intermediate ABR, %	147.6 ± 40.7	122.6 ± 23.1	149.6 ± 38.4	177.6 ± 49.6	3.182	0.061	0.020[b]

Values are mean ± SD or median (IQR). Group differences are assessed by one-way ANOVA, Fisher exact test, or Kruskal-Wallis H tests. [a]$P < 0.05$: the group difference assessed by one-way ANOVA was significant. [b]*P* for trend < 0.05: the linear association between continuous variables was significant, and the elevated $mPAP_{RHC}$ is evaluated by linear regression analysis. [c]$P < 0.05$: the group difference assessed by Kruskal-Wallis H test was significant.

AAD = ascending aorta diameter; ABR = pulmonary artery-bronchus ratio; IVCD = inferior vena cava diameter; LAD = left atrial diameter; LPAD = left pulmonary artery diameter; RAD = right atrial diameter; rPA = the ratio of MPAD to aorta diameter; RPAD = right pulmonary artery diameter; rRLA = the ratio of right to left atrial diameter; rSIVC = the ratio of superior to inferior vena cava diameter; SVCD = superior vena cava diameter; other abbreviations as in Tables 1 and 2.

artery diameter were 1.19 (95% CI: 1.03-1.38), 1.31 (95% CI: 1.01-1.71), and 1.30 (95% CI: 1.03-1.65) in HAPH patients, respectively ($P < 0.05$). Moreover, the ORs of rRLA, rPA, and left lower ABR were 1.09 (95% CI: 1.01-1.17), 1.14 (95% CI: 1.01-1.28), and 1.13 (95% CI: 1.02-1.25), respectively ($P < 0.05$). There was no significance in echocardiography measurements, such as TRPG, PASP, and LVEF (Table 5); these results were consistent with the correlation analysis.

NONINVASIVE ESTIMATION OF PULMONARY ARTERIAL PRESSURE. According to the results of correlation and logistic regression analysis, echocardiography continuous variables, and CTA variables with $r > 0.50$ and OR (95% CI) >1.00 were taken as the input variables of the estimation model. The stepwise multivariable linear regression showed the best diagnostic accuracy if left lower ABR and rRLA were included as covariates with the exclusion of right atrial diameter, inferior vena cava diameter, rPA, TRPG, and PASP, which provided superior diagnostic accuracy compared to each parameter alone (Figure 2A). The following model for noninvasive estimation of $mPAP_{RHC}$ was determined: $mPAP_{predicted} = -34 + 40 \times$ left lower ABR $+ 7 \times$ rRLA ($r = 0.907$, $R^2 = 0.823$, $P < 0.0001$) (Figure 2B). Standardized beta coefficients for left lower ABR and rRLA were 0.757 and 0.255, respectively. Partial regression plots showed good representation for selected variables, which could be incorporated into the estimation model as the main variables (Figure 2C).

After the model was established, Bland-Altman analysis was performed to verify the consistency of mPAP from the estimation model with that of RHC. Within the 95% limits of agreement, the average difference between the $mPAP_{predicted}$ and $mPAP_{RHC}$ was 1.75 mm Hg (Figure 2D). Area under the ROC curve values of $mPAP_{predicted}$, left lower ABR, and rRLA calculated by ROC curve were 0.952, 0.929, and 0.921, and cut-off values were 40 mm Hg, 1.61, and 1.43, respectively (Supplemental Figure 3). The sensitivity/specificity and positive/negative predictive value were shown in Supplemental Table 4.

PULMONARY VASCULAR REMODELING IN PREDICTED HAPH. To further confirm the consistent trend between the model and pathological damage of HAPH, collected lung tissues were divided into plateau residents and patients with HAPH according to the $mPAP_{predicted}$ and compared with the plain residents (Supplemental Table 5). Hematoxylin and eosin staining and immunohistochemistry staining against α-SMA were performed and representative PH vascular lesions were observed in HAPH patients based on $mPAP_{predicted}$ (Figure 3). Compared with plain residents, microvascular proliferation and fibrosis of intima were increased in plateau residents and were more pronounced in the plateau HAPH patients ($P < 0.01$) (Figure 3A). In addition, the anti-α-SMA immunohistostaining showed substantial muscularization of the pulmonary vasculature in predicted HAPH patients ($P < 0.01$) (Figure 3B). Interstitial thickening was

FIGURE 1 **Imaging Process in Pulmonary Arteriography and CTA/CT**

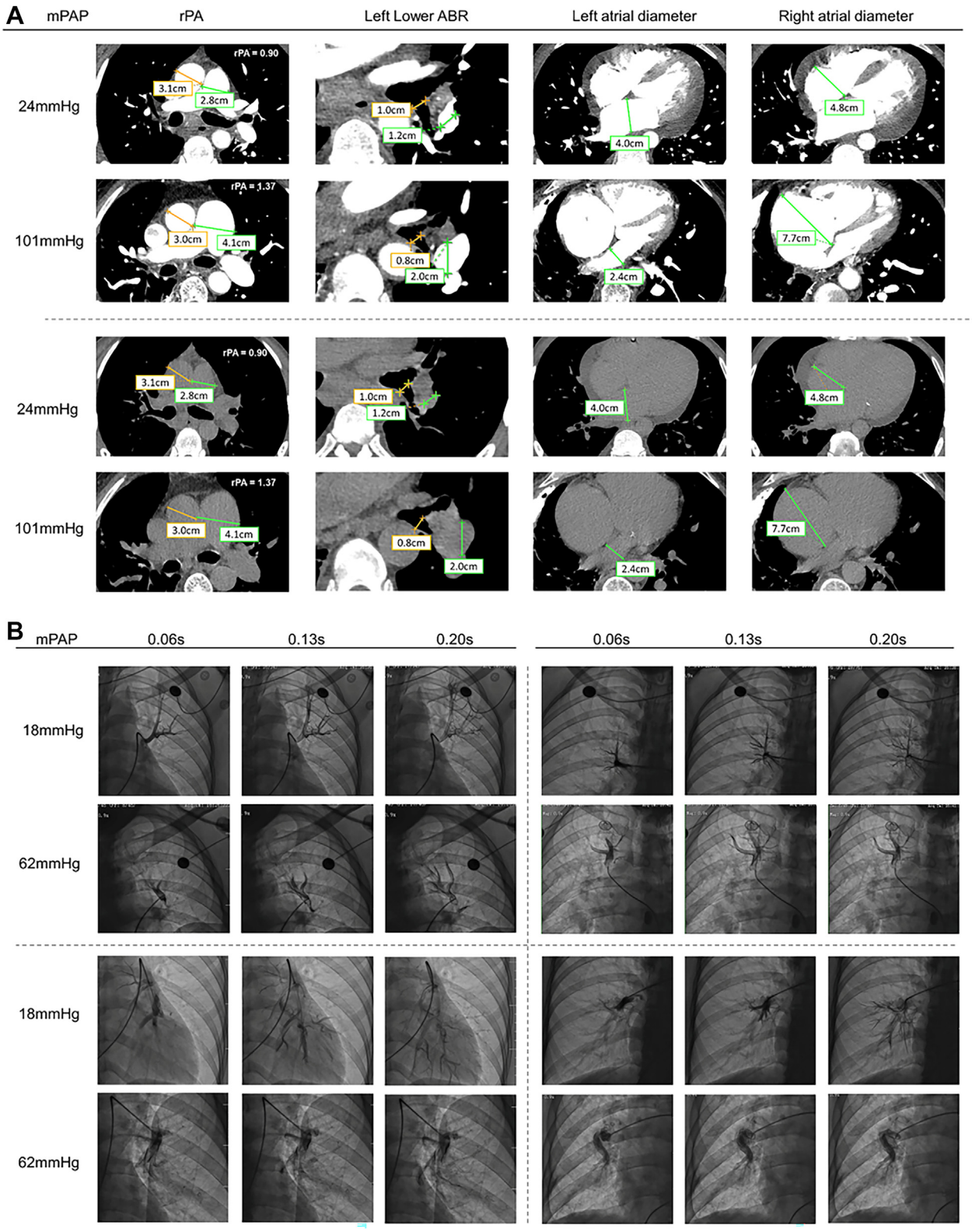

Continued on the next page

TABLE 4 Pearson's/Spearman's Correlation Coefficients Relating $mPAP_{RHC}$ to Measurements

	Mean ± SD or Median (IQR)	r	*P* Value
$mPAP_{RHC}$	45.76 ± 21.22	—	—
RAD, mm	64.08 ± 16.29	0.546	0.005[a]
LAD, mm	38.56 ± 9.09	-0.278	0.179
SVCD, mm	29.84 ± 8.70	0.516	0.008[a]
IVCD, mm	23.12 ± 6.01	0.617	0.001[a]
AAD, mm	32.96 ± 4.61	0.037	0.859
MPAD, mm	38.76 ± 7.18	0.559	0.004[a]
LPAD, mm	26.72 ± 4.75	0.407	0.043[a]
RPAD, mm	26.24 ± 4.88	0.383	0.059
rRLA	1.63 (1.20-2.02)	0.649	0.001[b]
rSIVC	1.32 ± 0.32	0.069	0.745
rPA	1.18 ± 0.20	0.583	0.002[a]
Left upper ABR	1.33 (1.15-1.50)	0.235	0.258
Left lower ABR	1.55 (1.35-1.86)	0.821	0.001[b]
Right upper ABR	1.48 ± 0.41	0.363	0.074
Right intermediate ABR	1.55 ± 0.40	0.287	0.165
TRPG	51.44 ± 24.35	0.469	0.018[a]
PASP, mm Hg	62.5 ± 24.69	0.439	0.028[a]
LVEF, %	63 (53-66)	0.279	0.176

[a]$P < 0.05$: the Pearson's correlation coefficient was significant; the correlation between independent variables and $mPAP_{RHC}$ was significant. [b]$P < 0.05$: the Spearman's correlation coefficient was significant; the correlation between independent variables and $mPAP_{RHC}$ was significant.

Abbreviations as in Tables 1 to 3.

also observed those predicted HAPH patients, and assumed as focal multiplication of alveolar capillaries, multiple layers within the alveolar septa at higher magnification (Figure 3C). The original data from the vessel wall thickness measurements are shown in Supplemental Table 6. The results show that HAPH patients with elevated $mPAP_{predicted}$ had significant vascular smooth muscle hyperplasia and alveolar septa thickening compared with that of the plain residents, suggesting a relatively high consistency of the prediction model and pathological alteration in PH patients.

DISCUSSION

This study focused on HAPH, one of the group 3 PH types with $mPAP_{RHC}$ >30 mm Hg, a PH subset which is more limited for diagnosis and treatment in plateau and has not yet drawn enough attention worldwide as of today.[12,19] This is the first study to show imaging characteristics of HAPH patients by multimodality imaging and demonstrate the pathological changes of lung tissue from plateau residents, which helps broaden the knowledge of HAPH (Central Illustration). In this research, elevated laboratory markers of HAPH patients related to the liver, kidney, and heart, and CTA showed enlarged right atrium and rRLA, both of which suggested the right heart insufficiency and played an auxiliary role in clinical diagnosis. Then, a regression model for the noninvasive prediction of $mPAP_{RHC}$ combining vascular, bronchial, and atrial diameter based on CTA was successfully established and showed good diagnostic value. In addition, the combination of left lower ABR and rRLA in the regression model provided superior diagnostic accuracy compared to each parameter alone. The angiography of HAPH patients suggested changes of ventilation/perfusion ratio in different lobes. The abnormal morphology and slowed blood flow were more obvious in the lower pulmonary artery and reflected increased circulation resistance, which led the compensatory lower pulmonary artery dilatation thus resulting in the increase of ABR (Supplemental Table 7).

In previous studies of pulmonary arterial pressure prediction, echocardiographic PASP was used in combination with other functional imaging modalities such as chest radiography, CT, and magnetic resonance imaging for model establishment.[20-26] However, magnetic resonance imaging was limited due to low availability and high cost, and echocardiographic PASP was not accurate compared with $mPAP_{RHC}$ in our study, with the difference of more than 40 mm Hg by echocardiography in some patients. It was also reported that residents in plateau were more likely to be associated with right ventricular insufficiency, whereas between-method differences of PASP and $mPAP_{RHC}$ in patients with right heart diseases were more obvious than in patients with left heart diseases.[27-29] The diseases spectrum, the high variability, and observer dependence of echocardiography might account for the inaccurate prediction of PASP in plateau.[11] Given that CTA provides more reliable data compared with echocardiography, it could be performed in patients with suspected PH and serve as a diagnostic algorithm for suspected PH.[1] In addition to assisting in the

FIGURE 1 Continued

(A) The diameter of main pulmonary artery, aorta, right atrium, left atrium, left lower pulmonary artery, and bronchus from a patient with high-altitude pulmonary hypertension (HAPH) and a plateau resident with normal mean pulmonary arterial pressure on right heart catheterization ($mPAP_{RHC}$) on CTA **(upper)** or CT **(lower)**; **(B)** The imaging process of pulmonary arteriography in a patient with HAPH and a plateau resident with normal $mPAP_{RHC}$. Left upper pulmonary artery **(upper left)**, right upper pulmonary artery **(upper right)**, left lower pulmonary **(lower left)**, and right lower pulmonary artery **(lower right)**. ABR = pulmonary artery-bronchus ratio; CT = computed tomography; CTA = computed tomography angiography; rPA = ratio of main pulmonary artery to aorta diameter.

diagnosis of HAPH, CTA provided information to rule out other lung or cardiac diseases related with PH, such as congenital heart disease, chronic thrombotic pulmonary disease, and other diseases easily misdiagnosed such as high-altitude pulmonary edema. Noninvasive prediction of PH based on CTA appeared to be a promising approach for translation into clinical routine, and several imaging indicators had been proved with predictive value, such as rPA, rRLA, and ABR.[30-34] Previous modeling studies based on CTA have converted the 1-dimensional diameter to 2-dimensional area calculation and 3-dimensional model establishment, but the practical clinical application was difficult in the plateau.[33,35] Therefore, the indicators selected in this study were calculated based on the parameters easily collected in the reading process and were more convenient for clinicians to make a preliminary diagnosis.

We confirmed the pathological changes of predicted HAPH based on $mPAP_{predicted}$, including fibrosis of intima, substantial vascular muscularization, interstitial thickening, and alveolar septa multiple layers formation. The thinning of the air-blood barrier reduced the resistance to gas diffusion, and

TABLE 5 Odds Ratios for HAPH Associated With Measurement

	Wald Chi-Square	*P* Value	Odds Ratio (95% CI)
RAD, mm	5.539	0.019[a]	1.193 (1.030-1.381)
LAD, mm	0.879	0.348	0.953 (0.861-1.054)
SVCD, mm	2.820	0.093	1.169 (0.974-1.403)
IVCD, mm	4.044	0.044[a]	1.311 (1.007-1.708)
AAD, mm	0.812	0.367	0.911 (0.744-1.116)
MPAD, mm	3.446	0.063	1.140 (0.993-1.310)
LPAD, mm	4.684	0.030[a]	1.302 (1.025-1.654)
RPAD, mm	0.785	0.375	1.086 (0.905-1.304)
rRLA, %	4.436	0.035[a]	1.086 (1.006-1.172)
rSIVC, %	0.020	0.887	0.998 (0.970-1.026)
rPA, %	4.612	0.032[a]	1.137 (1.011-1.278)
Left upper ABR, %	0.075	0.785	1.005 (0.970-1.041)
Left lower ABR, %	5.485	0.019[a]	1.128 (1.020-1.247)
Right upper ABR, %	3.108	0.078	1.029 (0.997-1.062)
Right intermediate ABR, %	3.142	0.076	1.032 (0.997-1.068)
TRPG, mm Hg	3.462	0.063	1.048 (0.998-1.101)
PASP, mm Hg	3.370	0.066	1.047 (0.997-1.099)
LVEF, %	0.555	0.456	1.036 (0.944-1.136)

[a]$P < 0.05$: the group difference assessed by univariate logistic regression test was significant.
HAPH = high-altitude pulmonary hypertension; other abbreviations as in Tables 2 and 3.

FIGURE 2 Noninvasive Estimation of Pulmonary Arterial Pressure

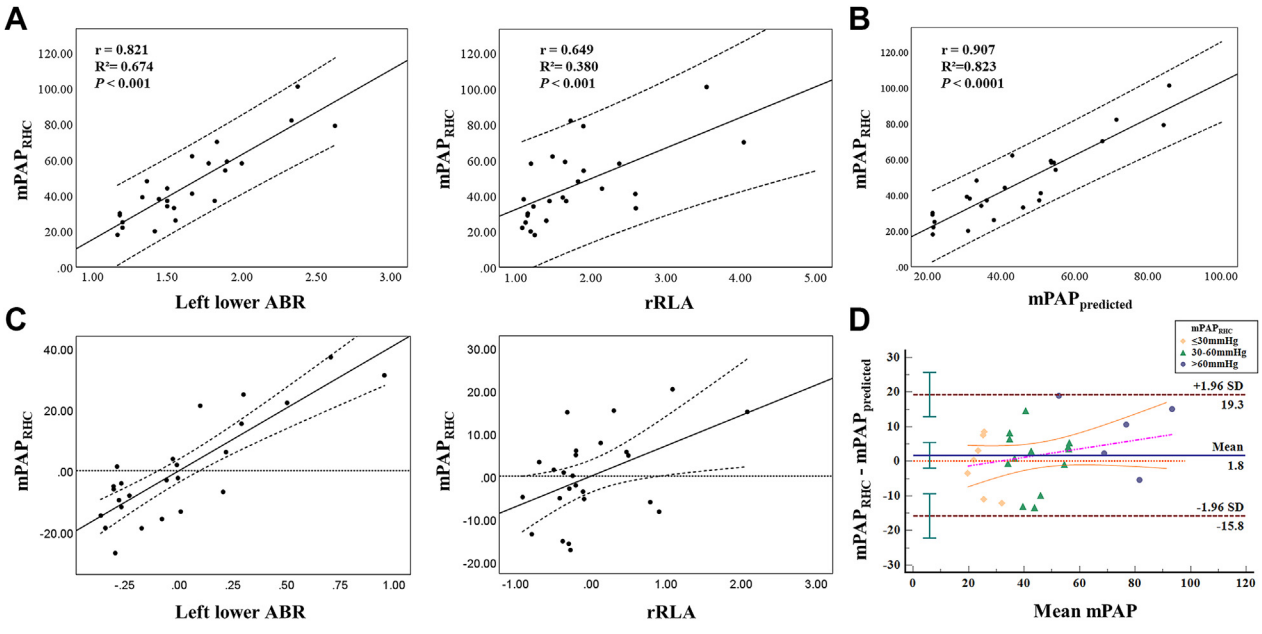

Multivariable linear regression and partial regression plot. **(A)** Correlation and 95% CI between left lower ABR, ratio of right to left atrial diameter (rRLA), and $mPAP_{RHC}$. **(B)** Correlation and 95% CI between $mPAP_{predicted}$ and $mPAP_{RHC}$. Noninvasive prediction model: $mPAP_{predicted} = -34 + 40 \times$ left lower ABR $+ 7 \times$ rRLA. **(C)** Partial regression plot (dependent variable: $mPAP_{RHC}$) of left lower ABR and rRLA. **Dashed line** indicates 95% CI. **(D)** Bland-Altman analysis (figures are rounded). Mean mPAP was calculated as ($mPAP_{predicted} + mPAP_{RHC}$) / 2. Mean difference between $mPAP_{predicted}$ and $mPAP_{RHC}$ **(middle blue line)** is 1.75 mm Hg with a 95% CI. of -1.95 to 5.45 **(yellow lines)**. Abbreviations as in Figure 1.

FIGURE 3 Pathological Analysis in Patients Predicted With HAPH

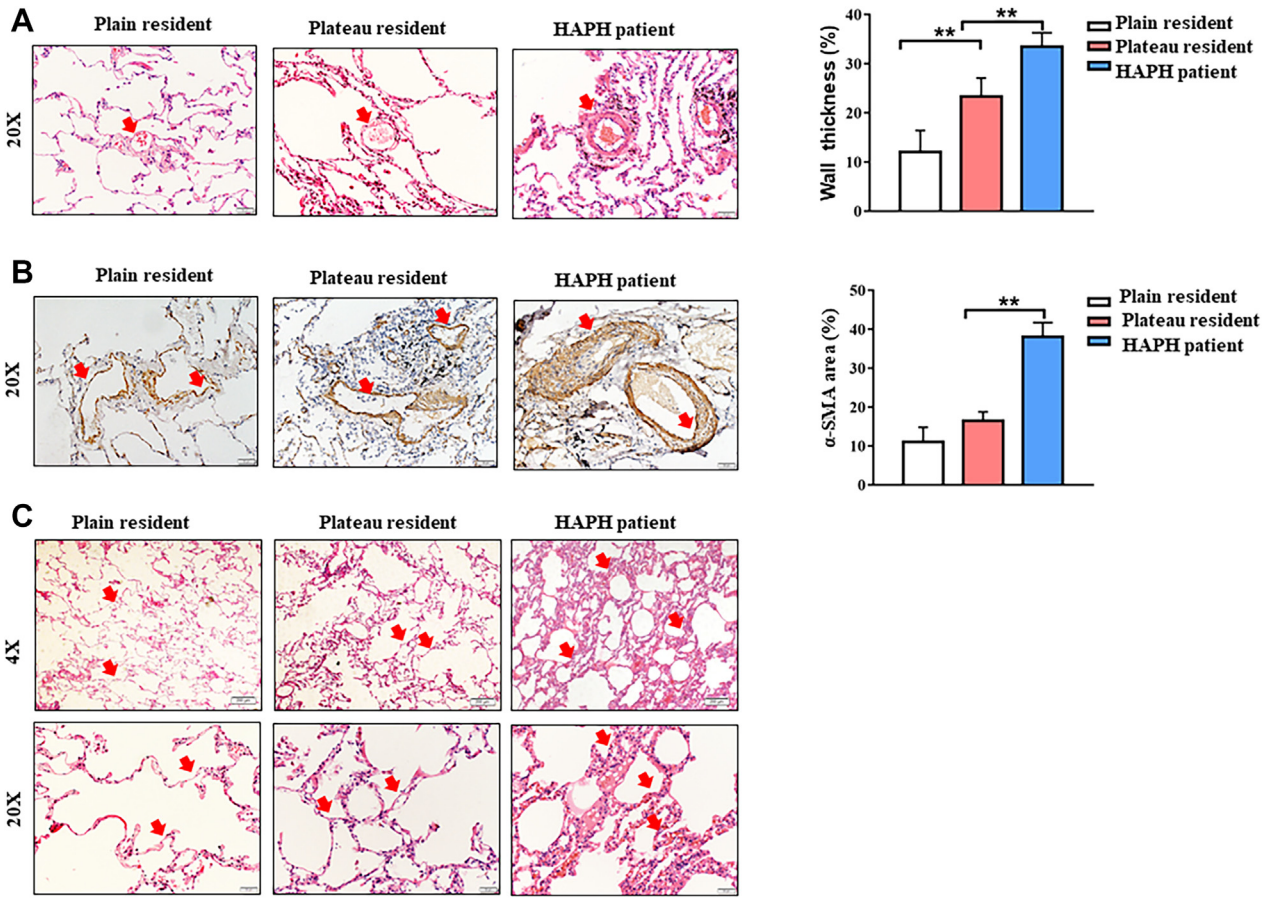

(A) Quantitative analysis of vascular thickness in hematoxylin and eosin staining **(arrow).** Microvascular proliferation, fibrosis of intima. **Scale bars,** 50 μm. **(B)** Muscularization of the pulmonary vasculature in immunohistochemistry staining **(arrow)** and quantitative analysis reflected by α-smooth muscle actin. **Scale bars,** 50 μm. Data are expressed as mean ± SD. $^{**}P < 0.01$. Data were analyzed using one-way analysis of variance. **(C) Upper**: Interstitial thickening (original magnification ×4), focal multiplication of alveolar capillaries **(arrow). Scale bars,** 200 μm. **Lower:** multiple layers formed within the alveolar septa at higher magnification (original magnification, ×20) **(arrow). Scale bars,** 50 μm.

the failure of compensatory thinning of alveolar septa to adapt to altitude enhancement may be one of the mechanisms underlying HAPH.[36] The pathological changes, especially the media thickening, were similar to pulmonary arterial hypertension.[37] The identification of factors triggering proliferation of pulmonary arterial smooth muscle cells (the main cellular components of media hypertrophy) in particular under the stress of hypoxia would provide therapeutic targets against pulmonary vascular remodeling in HAPH apart from the basic oxygen therapy.[38]

STUDY LIMITATIONS. The sample size was relatively small in our study, with 25 patients enrolled. Nevertheless, variables were analyzed in different aspects before the process of model establishment, and the Bland-Altman analysis, linear regression, and partial regression plot were used to evaluate the consistency of the predicting method and RHC in terms of mPAP assessment and the quality of selected variables. In addition, typical vascular remodeling of PH was also found in HAPH patients diagnosed with $mPAP_{predicted}$, which further proved the reliability of this model.[39] With the application of RHC in plateau, more suspected HAPH patients will be included for model correction, and more prospective studies are warranted to further confirm our findings in the future.

CONCLUSIONS

In this study, a noninvasive mPAP estimation model in HAPH was established based on the pulmonary

CENTRAL ILLUSTRATION **Brief Flow Chart and Prediction Model of High-Altitude Pulmonary Hypertension Based on Computed Tomography Angiography**

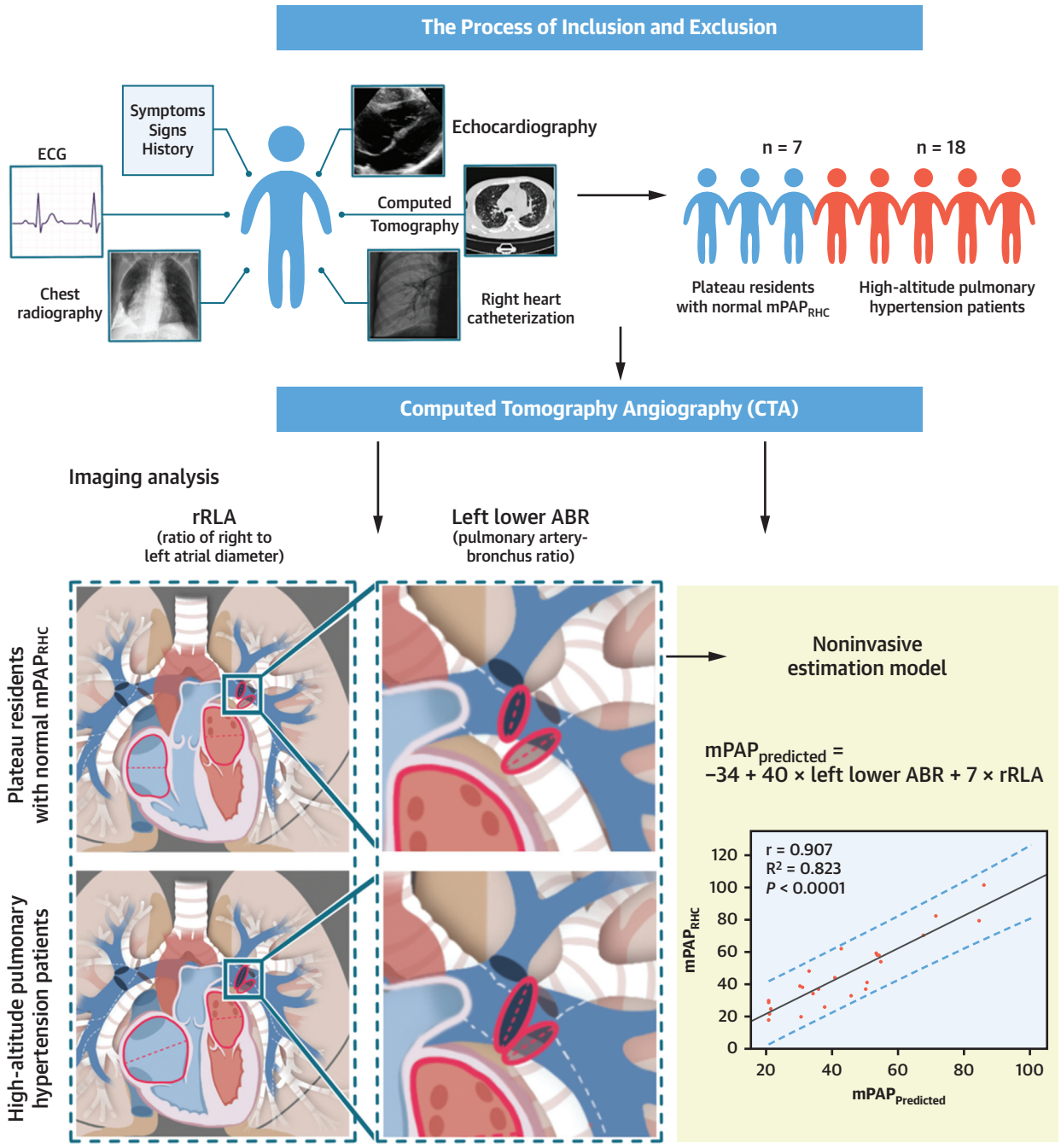

Zeng Y, et al. JACC: Asia. 2022;2(7):803–815.

Computed tomography angiography showed dilated pulmonary vessels, enlarged right atrium, and compressed left atrium in patients with high-altitude pulmonary hypertension. **Left lower** pulmonary artery-bronchus ratio (ABR) and ratio of right to left atrial diameter (rRLA) were calculated to further establish a noninvasive prediction model for mean pulmonary arterial pressure (mPAP). ECG = electrocardiogram; RHC = right heart catheterization.

JACC: ASIA, VOL. 2, NO. 7, 2022
DECEMBER 2022:803–815

ABR and the rRLA in CTA, and was confirmed by gold standard RHC and pathology. The estimation model reduced the insufficiency of echocardiography in predicting pulmonary artery pressure and provided a more accurate method for early diagnosis of HAPH in plateau.

ACKNOWLEDGMENT The authors thank Yi Yan (German Centre for Cardiovascular Research, PartnerSite Munich Heart Alliance, Munich) for assistance in potential mechanism and revision, and patients who participated in this study.

FUNDING SUPPORT AND AUTHOR DISCLOSURES

Supported by the National Natural Science Foundation of China (81900239, 82070230, 91939101) and the Clinical Research Plan of SHDC (No. SHDC2020CR4019). The authors have reported that they have no relationships relevant to the contents of this paper to disclose.

ADDRESS FOR CORRESPONDENCE: Dr Wenhui Peng, Department of Cardiology, Shanghai Tenth People's Hospital, Tongji University School of Medicine, 301 Middle Yanchang Road, Shanghai 200072, China. E-mail: pwenhui@tongji.edu.cn. OR Dr. Yong Liu, Department of Radiology, Shanghai Tenth People's Hospital, Tongji University School of Medicine, 301 Middle Yanchang Road, Shanghai 200072, China. E-mail: ly777dragon@sina.com.

PERSPECTIVES

COMPETENCY IN MEDICAL KNOWLEDGE: The imaging characteristics of HAPH patients included: 1) slow blood flow and coral signs in the lower pulmonary artery in pulmonary arteriography; and 2) serious dilated pulmonary vessels, enlarged right atrium, and compressed left atrium in CTA. Echocardiographic PASP was not accurate for $mPAP_{RHC}$ prediction in HAPH patients associated with right ventricular insufficiency.

TRANSLATIONAL OUTLOOK 1: For potential HAPH patients, CTA provided information to rule out other lung or cardiac diseases related with PH and diseases easily misdiagnosed, and further predicted $mPAP_{RHC}$ based on the ARB and the atrial ratio.

TRANSLATIONAL OUTLOOK 2: For HAPH patients intolerant of contrast agents during the CTA procedure, the measurements of CT may reduce the accuracy of prediction. This predictive model should be corrected in a feedback manner to improve its diagnostic accuracy with the increase of confirmed cases in the future.

REFERENCES

1. Galiè N, Humbert M, Vachiery JL, et al. 2015 ESC/ERS guidelines for the diagnosis and treatment of pulmonary hypertension. *Eur Respir J*. 2015;46:903–975.

2. Morrison D, Goldman S, Wright AL, et al. The effect of pulmonary hypertension on systolic function of the right ventricle. *Chest*. 1983;84:250–257.

3. Farber HW, Gibbs S. Under pressure: pulmonary hypertension associated with left heart disease. *Eur Respir Rev*. 2015;24:665–673.

4. Bärtsch P, Swenson ER. Acute high-altitude illnesses. *N Engl J Med*. 2013;368:2294–2302.

5. Moore LG. Human genetic adaptation to high altitude. *High Alt Med Biol*. 2001;2:257–279.

6. Lei S, Sun Z, He X, et al. Clinical characteristics of pulmonary hypertension patients living in plain and high-altitude regions. *Clin Respir J*. 2019;13:485–492.

7. Naeije R, Huez S, Lamotte M, et al. Pulmonary artery pressure limits exercise capacity at high altitude. *Eur Respir J*. 2010;36:1049–1055.

8. Villafuerte FC, Corante N. Chronic mountain sickness: clinical aspects, etiology, management, and treatment. *High Alt Med Biol*. 2016;17:61–69.

9. Gali N, Hoeper MM, Humbert M, et al. Guidelines for the diagnosis and treatment of pulmonary hypertension. *Eur Heart J*. 2009;30:2493–2537.

10. Xu XQ, Jing ZC. High-altitude pulmonary hypertension. *Eur Respir Rev*. 2009;18:13–17.

11. Fisher MR, Forfia PR, Chamera E, et al. Accuracy of Doppler echocardiography in the hemodynamic assessment of pulmonary hypertension. *Am J Respir Crit Care Med*. 2009;179:615–621.

12. León-Velarde F, Maggiorini M, Reeves JT, et al. Consensus statement on chronic and subacute high altitude diseases. *High Alt Med Biol*. 2005;6:147–157.

13. Filipek MS, Gosselin MV. Multidetector pulmonary CT angiography: advances in the evaluation of pulmonary arterial diseases. *Semin Ultrasound CT MR*. 2004;25:83–98.

14. Mitchell C, Rahko PS, Blauwet LA, et al. Guidelines for performing a comprehensive transthoracic echocardiographic examination in adults: recommendations from the American Society of Echocardiography. *J Am Soc Echocardiogr*. 2019;32:1–64.

15. Zoghbi WA, Adams D, Bonow RO, et al. ASE guidelines and standards recommendations for noninvasive evaluation of native valvular regurgitation a report from the American Society of Echocardiography Developed in Collaboration with the Society for Cardiovascular Magnetic Resonance. *J Am Soc Echocardiogr*. 2017;30:303–371.

16. Augustine DX, Coates-Bradshaw LD, Willis J, et al. Echocardiographic assessment of pulmonary hypertension: a guideline protocol from the British Society of Echocardiography. *Echo Res Pract*. 2018;5:G11–G24.

17. Rosenkranz S, Preston IR. Right heart catheterisation: best practice and pitfalls in pulmonary hypertension. *Eur Respir Rev*. 2015;24:642–652.

18. Mirrakhimov AE, Strohl KP. High-altitude pulmonary hypertension: an update on disease pathogenesis and management. *Open Cardiovasc Med J*. 2016;10:19–27.

19. Moore LG, Niermeyer S, Zamudio S. Human adaptation to high altitude: regional and life-cycle perspectives. *Yearb Phys Anthropol*. 1998;41:25–64.

20. Yang S, Lei S, Peng F, et al. Detection of pulmonary hypertension by combining echocardiography and chest radiography. *Acad Radiol*. 2022;(Suppl 2):S23–S30.

21. Devaraj A, Wells AU, Meister MG, et al. Detection of pulmonary hypertension with multidetector CT and echocardiography alone and in combination. *Radiology*. 2010;254:609–616.

22. Devaraj A, Loveridge R, Bosanac D, et al. Portopulmonary hypertension: improved detection using CT and echocardiography in combination. *Eur Radiol*. 2014;24:2385–2393.

23. Albers J, Ister D, Kayhan N, et al. Postoperative non-invasive assessment of pulmonary vascular resistance using Doppler echocardiography. *Interact Cardiovasc Thorac Surg*. 2011;13:579–584.

24. Ley S, Kreitner KF, Fink C, et al. Assessment of pulmonary hypertension by CT and MR imaging. *Eur Radiol*. 2004;14:359–368.

25. Swift AJ, Rajaram S, Hurdman J, et al. Noninvasive estimation of PA pressure, flow, and resistance with CMR imaging: derivation and prospective validation study from the ASPIRE registry. *J Am Coll Cardiol Img*. 2013;6:1036–1047.

26. Johns CS, Rajaram S, Capener DA, et al. Non-invasive methods for estimating mPAP in COPD using cardiovascular magnetic resonance imaging. *Eur Radiol*. 2018;28:1438–1448.

27. Naeije R. Physiological adaptation of the cardiovascular system to high altitude. *Prog Cardiovasc Dis*. 2010;52:456–466.

28. Hackett PH, Roach RC. High-altitude illness. *N Engl J Med*. 2001;345:107–114.

29. Finkelhor RS, Lewis SA, Pillai D. Limitations and strengths of doppler/echo pulmonary artery systolic pressure-right heart catheterization correlations: a systematic literature review. *Echocardiography*. 2015;32:10–18.

30. Kuriyama K, Gamsu G, Stern RG, et al. CT-determined pulmonary artery diameters in predicting pulmonary hypertension. *Invest Radiol*. 1984;19:16–22.

31. Gerges M, Gerges C, Lang IM. Advanced imaging tools rather than hemodynamics should be the primary approach for diagnosing, following, and managing pulmonary arterial hypertension. *Can J Cardiol*. 2015;31:521–528.

32. Corson N, Armato SG, Labby ZE, et al. CT-based pulmonary artery measurements for the assessment of pulmonary hypertension. *Acad Radiol*. 2014;21:523–530.

33. Huisin't Veld AE, Van Vliet AG, Spruijt OA, et al. CTA-derived left to right atrial size ratio distinguishes between pulmonary hypertension due to heart failure and idiopathic pulmonary arterial hypertension. *Int J Cardiol*. 2016;223:723–728.

34. Woodring JH. Pulmonary artery-bronchus ratios in patients with normal lungs, pulmonary vascular plethora, and congestive heart failure. *Radiology*. 1991;179:115–122.

35. Melzig C, Wörz S, Egenlauf B, et al. Combined automated 3D volumetry by pulmonary CT angiography and echocardiography for detection of pulmonary hypertension. *Eur Radiol*. 2019;29:6059–6068.

36. Hsia CCW, Hyde DM, Weibel ER. Lung structure and the intrinsic challenges of gas exchange. *Compr Physiol*. 2016;6:827–895.

37. Humbert M, Guignabert C, Bonnet S, et al. Pathology and pathobiology of pulmonary hypertension: state of the art and research perspectives. *Eur Respir J*. 2019;53(1):1801887.

38. He YY, Xie XM, Zhang H Da, et al. Identification of hypoxia induced metabolism associated genes in pulmonary hypertension. *Front Pharmacol*. 2021;12:753727.

39. Tuder RM, Archer SL, Dorfmüller P, et al. Relevant issues in the pathology and pathobiology of pulmonary hypertension. *J Am Coll Cardiol*. 2013;62(suppl 25):D4–D12.

KEY WORDS computed tomography, plateau, pulmonary arterial pressure, pulmonary artery-bronchus ratio

APPENDIX For supplemental tables and figures, please see the online version of this paper.